Mobility of Nanosized Cerium Dioxide and Polymeric Capsules in Quartz and Loamy Sands Saturated with Model and Natural Groundwaters

ADAMO RICCARDO PETOSA, CAROLIN ÖHL, FARAZ RAJPUT, and NATHALIE TUFENKJI[*]

Department of Chemical Engineering, McGill University,
3610 University St., Montreal, Quebec, Canada H3A 2B2

*Corresponding Author: Nathalie Tufenkji
    Phone: (514) 398-2999; Fax: (514) 398-6678; E-mail: nathalie.tufenkji@mcgill.ca

Abstract

The environmental and health risks posed by emerging engineered nanoparticles (ENPs) released into aquatic environments are largely dependent on their aggregation, transport, and deposition behavior. Herein, laboratory-scale columns were used to examine the mobility of polyacrylic acid (PAA)-coated cerium dioxide nanoparticles (nCeO$_2$) and an analogous nanosized polymeric capsule (nCAP) in water saturated quartz sand or loamy sand. The influence of solution ionic strength (IS) and cation type (Na$^+$, Ca^{2+}, or Mg^{2+}) on the transport potential of these ENPs was examined in both granular matrices and results were also compared to measurements obtained using a natural groundwater. ENP suspensions were characterized using dynamic light scattering and nanoparticle tracking analysis to establish aggregate size, and laser Doppler electrophoresis to determine ENP electrophoretic mobility. Regardless of IS, virtually all nCeO$_2$ particles suspended in NaNO$_3$ eluted from the quartz sand-packed columns. In contrast, heightened nCeO$_2$ and nCAP particle retention and dynamic (time-dependent) transport behavior was observed with increasing concentrations of the divalent salts and in the presence of natural groundwater. Enhanced particle retention was also observed in loamy sand in comparison to the quartz sand, emphasizing the need to consider the nature of the aqueous matrix and granular medium in evaluating contamination risks associated with the release of ENPs in natural and engineered aquatic environments.

1. Introduction

Engineered nanoparticles (ENPs) exhibit appealing physicochemical properties that are absent in larger particles with equivalent chemical compositions (Auffan et al., 2009, Klaine et al., 2008). Consequently, ENPs of all types (e.g., carbon nanotubes, metals and metal oxides, semiconductors, polymers) are being incorporated into a growing number of consumer products. For example, nanosized titanium dioxide (nTiO$_2$) is employed in the production of sunscreens and paint, zinc oxide (nZnO) is used in cosmetics and solar cells, and iron oxides are incorporated into pigments and used in biological applications (Ju-Nam and Lead, 2008, Klaine et al., 2008). Comprehensive reviews of existing ENP types and their applications are available in the literature (Ju-Nam and Lead, 2008, Klaine et al., 2008). An inventory of consumer products containing ENPs has also been developed by the Woodrow Wilson International Center for Scholars (available at http://www.nanotechproject.org/).

Nanosized cerium dioxide (nCeO$_2$) is currently employed in several applications. It can serve as a polishing agent when manufacturing glass and can serve as a capacitor and semiconductor (Johnson and Park, 2012). Given that nCeO$_2$ protects against the oxidative stress caused by reactive oxygen species, medical applications have also been described. These include the use of nCeO$_2$ as an antioxidant to treat retinal disorders such as glaucoma (García et al., 2011). Since nCeO$_2$ effectively absorbs ultraviolet radiation, it is used in the production of sunscreens and UV blocking agents (Cassee et al., 2011). Surface reactive properties also make nCeO$_2$ a useful exhaust gas catalyst (Cassee et al., 2011, Van Hoecke et al., 2011).

Exposure to ENPs can occur at all stages of the particle lifecycle, including fabrication and processing, product usage and disposal (Wiesner and Bottero, 2007). Many nCeO$_2$ applications are dispersive in nature, increasing the risk for exposure and heightened interactions

3

with a variety of environmental media (Cassee et al., 2011). The release of nCeO$_2$ particles employed as UV blocking agents or diesel fuel additives may threaten aquatic and sediment dwelling organisms (Van Hoecke et al., 2011). Beyond that, ENPs entering soil environments may reach groundwater aquifers, potentially contaminating drinking water supplies and causing unknown health, safety and environmental issues (Klaine et al., 2008). Once introduced into natural subsurface environments or engineered water treatment processes, particle aggregation, transport and deposition behavior will play a major role in determining nCeO$_2$ fate, bioavailability and the likelihood for human exposure. Thus, a comprehensive understanding of nCeO$_2$ transport and deposition behavior in water saturated granular systems is required for the protection of environmental and public health.

Well-controlled laboratory experiments using columns packed with different granular matrices can be useful for drawing links between collector (grain) properties and the mobility of released ENPs in water saturated granular environments (Kretzschmar et al., 1994, Petosa et al., 2010, Quevedo and Tufenkji, 2012). A number of studies have examined the transport and deposition of ENPs in quartz sand-packed columns, providing useful insights on the effects of environmental factors such as water chemistry, grain size, particle size, and porewater velocities on ENP mobility (Petosa et al., 2010). However, little is known regarding the transport and deposition of nCeO$_2$ in water saturated granular environments (Li et al., 2011b, Liu et al., 2012).

Published nCeO$_2$ transport studies have focused on the transport of bare particles suspended in monovalent salt solutions (namely, NaCl). In considering the effect of pH and IS on nCeO$_2$ deposition on sand, Li *et al.* observed increased particle retention under acidic conditions (pH 3) and with increasing NaCl IS (Li et al., 2011b). Liu *et al.* investigated nCeO$_2$

deposition in sand-packed columns and using a quartz crystal microbalance with dissipation (QCM-D). In NaCl (pH 6.5 and 8), far more nCeO$_2$ deposition was observed in the packed columns than on silica QCM-D sensors, likely due to physical straining as a result of ENP aggregation and heterogeneities on the quartz sand collectors. Heightened nCeO$_2$ mobility in the packed columns was observed in the presence of organic matter (Liu et al., 2012). The transport of nCeO$_2$ in the presence of divalent salt solutions (e.g., CaCl$_2$ and MgCl$_2$) and natural groundwater matrices has not been reported in the literature. Furthermore, studies investigating nCeO$_2$ transport in granular matrices other than quartz sand are not available.

While the types of granular materials encountered in the natural subsurface environment can vary broadly (Kretzschmar et al., 1994), few studies have investigated the transport behavior of selected ENPs in media other than glass beads and quartz sand (Jaisi and Elimelech, 2009, Petosa et al., 2010). Previously, our group has shown that the retention of two different carboxyl-terminated quantum dots (QDs) and a carboxylated polystyrene latex nanoparticle can be enhanced by at least one order of magnitude in a loamy sand versus a quartz sand of comparable mean grain size (Quevedo and Tufenkji, 2012). Interestingly, the 3 different ENPs exhibit similar mobility in the quartz sand, but distinct transport behaviors in the loamy sand. This suggests that differences in the affinities of the polymer-coated ENPs for specific soil components can control their fate in subsurface environments. Jaisi and Elimelech investigated the transport of carboxyl-functionalized single-walled carbon nanotubes (SWCNTs) in columns packed with a complex granular matrix; namely, a sandy clay loam. Their study found SWCNT transport to be governed by physical straining, likely due to the combined effects of a very large NP aspect ratio, NP aggregation in solution and variability in soil particle size, porosity and permeability (Jaisi and Elimelech, 2009).

The purpose of this work is to systematically investigate the mobility of a polyacrylic acid (PAA)-coated nCeO$_2$ particle in water-saturated quartz sand and loamy sand matrices. Natural and artificial groundwaters are used to study the effect of electrolyte species and ionic strength (IS) on selected particle properties (i.e., aggregate size and surface potential) and transport potential. This study is the first to consider the effects of more complex granular materials and water chemistries on the transport behavior of nCeO$_2$ in water saturated porous media. Moreover, the behavior of the PAA-coated nCeO$_2$ is compared to that of analogous PAA-based nanocapsules (nCAPs) to assess whether both particle types exhibit similar transport potentials. The nCAPs employed herein were designed to serve as water dispersible polymeric nanocapsules in agricultural applications, providing a further incentive to examine their behavior in model subsurface environments.

2. Materials and Methods

2.1 Natural groundwater characterization

Natural groundwater, originating from a domestic well in the township of North Glengarry, Ontario, was thoroughly characterized (methods and results are included in the Supporting Information, Table S1 and Figure S1).

2.2 Granular collector surface characterization

Quartz sand (-50 +70 mesh size, d_{50}=256 µm, Sigma-Aldrich) and loamy sand (d_{50}=225 µm) acquired at a 35 cm depth from an Agriculture and Agri-Food Canada (AAFC) farm plot located in St-Augustin-de-Desmaures, QC, were employed as granular materials in this study. An electrokinetic analyzer (Anton Paar Electro Kinetic Analyzer) was used to determine the surface

6

(zeta) potential of the quartz sand for the experimental conditions considered herein (Supplementary Material, Table S2). Further collector characterization details are presented in the Supplementary Material and described elsewhere (Quevedo and Tufenkji, 2012).

2.3 Nanoparticle suspension preparation

Suspensions were prepared using polymer-coated $n\text{CeO}_2$ (Batch Number: PB 54) and $n\text{CAP}$ (Batch Number: PB 67) powders (Vive Crop Protection). According to the manufacturer, the $n\text{CeO}_2$ particles (cubic crystal structure) have a nominal size of 1-10 nm (TEM) and are coated with partially crosslinked PAA. The composition of the empty $n\text{CAPs}$ is analogous to that of the polymer-coating on the ceria particles (without the metal oxide core). The $n\text{CeO}_2$ and $n\text{CAP}$ synthesis is based on counter-ion induced polyelectrolyte collapse (Coulter et al., 2010). The PAA (polyelectrolyte) employed in producing the $n\text{CeO}_2$ coating and $n\text{CAP}$ particles has a 345 kDa weight average molecular weight (M_w). Furthermore, M_w for the $n\text{CAPs}$ is 113 kDa by gel permeation chromatography (GPC). Details regarding $n\text{CeO}_2$ purity and preparation of ENP suspensions are provided in the Supplementary Material. Briefly, a particle concentration of 100 mg/L was employed in all experiments. Experiments with $n\text{CeO}_2$ were conducted in natural groundwater or in artificial electrolyte solutions at IS ranging from 0.1 to 1 M sodium nitrate (NaNO_3), 0.33 to 10 mM calcium chloride (CaCl_2) and 0.33 to 12 mM magnesium chloride (MgCl_2). The $n\text{CAP}$ suspensions were prepared in CaCl_2 (0.33 to 20 mM) or natural groundwater. Suspension pH was stabilized using 1 mM MOPS and adjusted to pH 8 using NaOH.

2.4 Nanoparticle characterization

Particle electrophoretic mobilities (EPMs) were determined by laser Doppler electrophoresis (ZetaSizer Nano ZS, Malvern). All EPM measurements were performed at 25°C, with an applied electrical field (E) of 4.9±0.1 V/m. Particle hydrodynamic diameters were determined by DLS (d_{DLS}) using a Zetasizer Nano ZS (Malvern) and by nanoparticle tracking analysis (NTA, d_{NTA}) (Nanosight LM10+LM14, Wiltshire, UK). At least six independent replicate samples were analyzed using DLS and NTA.

2.5 Nanoparticle transport and deposition studies

ENP transport studies were performed using glass columns (16 mm inner diameter, GE Life Sciences) packed with quartz sand or loamy sand. Packed-bed porosities were 0.37 and 0.44 for the quartz and loamy sands, respectively. Prior to use, the quartz sand was prepared as previously described (Pelley and Tufenkji, 2008) and then soaked in background electrolyte for a minimum of 16 hours before wet packing into a glass column to a height of 14 cm. Gentle vibration was used to avoid air entrapment within the packed bed, ensure uniform packing, and minimize any possible layering of the quartz sand. Prior to injecting the suspended ENPs into the quartz sand packed column, 10 pore volumes (PVs) of background electrolyte were pumped through the column.

Before use, the loamy sand was dried in an oven at 105°C for 8 hours. All clumps in the dried soil were gently crushed using a ceramic pestle. With some modifications, loamy sand-packed columns were prepared as previously described (Jaisi and Elimelech, 2009, Kretzschmar et al., 1997) to a height of 7 cm. Briefly, loamy sand was dry-packed into a glass column. The column was then gently vibrated for 60 s to achieve uniform packing and purged with CO_2 at

low pressure (in the upward direction) for 20 minutes to improve water saturation. Next, the packed column was saturated with 20 mM $CaCl_2$ solution (upward direction, 0.2 mL/min flow rate) to stabilize the soil colloids. Once saturated, the column was further conditioned with 20 mM $CaCl_2$ at gradually increasing flow rates (stepwise from 0.2 to 1.3 mL/min) over the course of 1 hour. Next, an additional 40 PVs of $CaCl_2$ were added to the column, followed by 500 PVs of background electrolyte (both in the upward direction, 1.3 mL/min flow rate). Prior to the transport experiments, an additional 15 PVs of electrolyte were added (downward direction, 1.3 mL/min), followed by 1 PV at 0.4 mL/min. Beyond equilibration, the experimental procedure was identical for quartz and loamy sand-packed columns. Consistent packing of both column types was confirmed using 10 mM KNO_3 tracer experiments (data not shown).

For all column experiments, a 0.4 mL/min flow rate (equivalent to a Darcy velocity of 2.86 m/day) was employed. At least 3 PVs of ENP suspensions were injected, followed by particle-free electrolyte. Influent (C_0) and effluent (C) particle concentrations were tracked online using a UV-visible spectrophotometer (Agilent 8453) equipped with a 1 cm flow-through cell. The nCeO$_2$ particles were monitored at a wavelength of 300 nm in natural groundwater and divalent salts and at 320 nm in $NaNO_3$. The nCAPs were monitored at 210 nm. Very reproducible deposition data was obtained and all particle breakthrough curves presented are the average of at least 2 column experiments. At the highest $NaNO_3$ IS (0.5 and 1 M), nCeO$_2$ breakthrough curves were determined by inductively coupled plasma mass spectrometry (ICP-MS, Agilent 7500ce) using HNO_3-digested effluent samples.

2.6 Interpretation of ENP Transport Behavior

Particle transport behavior under the different experimental conditions was interpreted quantitatively using the particle attachment efficiency (α). All α values are calculated using the colloid filtration theory (Yao et al., 1971):

$$\alpha = -\frac{2}{3}\frac{d_{50}}{(1-\varepsilon)L\eta_0}\ln\left(\frac{C}{C_0}\right) \tag{1}$$

Here, d_{50} is the mean collector grain diameter, ε is the packed-bed porosity, L is the packed-bed length and C/C_0 corresponds to the normalized particle concentration at the column effluent. The value of C/C_0 used in eq 1 was determined in two ways: (i) by averaging measured values between 1.8-2 PVs and (ii) by numerical integration of the area under each measured particle breakthrough curve. Values of the single-collector contact efficiency, η_0, were determined using the Tufenkji-Elimelech correlation (Tufenkji and Elimelech, 2004).

3. Results and Discussion

3.1 Particle and quartz sand surface potential

Under the experimental conditions used here (pH 8), the EPMs of nCeO$_2$ and nCAP particles are negative (Table 1) due to the carboxylic acid groups present on the PAA chains. The experimentally determined point of zero charge (pH$_{zpc}$) for the nCeO$_2$ and nCAP particles is below pH 2 (Figure S2). In the natural groundwater, the nCeO$_2$ and nCAP EPMs are -1.2 and -0.87 μmcmV^{-1}s^{-1}, respectively (Table 1). Our measurement for nCeO$_2$ in groundwater is very comparable to that reported by Keller *et al.* (Keller et al., 2010) for nCeO$_2$ rods (67 × 8 nm nominal size, Meliorum Technologies): -1.1 μmcmV^{-1}s^{-1} in Santa Paula groundwater (pH 7.9) and -1.1 μmcmV^{-1}s^{-1} in Santa Clara river water (pH 8.33). While there is no indication that the

particles utilized by Keller *et al.* had a polymer coating such as the PAA utilized in the present study, the presence of organic carbon (considered to be a surrogate for natural organic matter) in the aquatic matrices was found to result in negative EPMs. Furthermore, increasing IS was found to result in less negative EPMs due to surface charge neutralization (Keller et al., 2010). As observed by Keller *et al.*, nCeO$_2$ EPMs become less negative with increasing IS in the monovalent and divalent salt solutions utilized herein (Table 1). EPM values for nCeO$_2$ range from -2.7 to -1.4 μmcmV^{-1}s^{-1} when the solution IS varies between 0.33 to 10 mM CaCl$_2$, from -2.7 to -0.79 μmcmV^{-1}s^{-1} when the solution IS varies between 0.33 to 12 mM MgCl$_2$ and from -1.1 to -0.57 μmcmV^{-1}s^{-1} when the salt concentration is increased from 100 to 500 mM NaNO$_3$ (Table 1). Likewise, nCAP particle EPM decreases from -2.3 to -1.0 μmcmV^{-1}s^{-1} when the solution IS increases from 0.33 to 20 mM CaCl$_2$ (Table 1).

Table 1. Measured hydrodynamic diameter and electrophoretic mobility (EPM) for *n*CeO2 and *n*CAP particles*

Particle	Ionic Strength (mM NaNO3)	Ionic Strength (mM CaCl2)	Ionic Strength (mM MgCl2)	Natural Groundwater	dDLS (nm)	PDI (for DLS)	dNTA (nm)	EPM (µmcmV-1s-1)	αDLS, quartz sand	αDLS, loamy sand
	100			Influent	54 ± 12.6	0.43	176 ± 28.4	-1.12 ± 0.093	5.2×10-4 ± 5.9×10-4	0.014 ± 1.8×10-3
				Effluent	57 ± 4.0	0.75		-1.06 ± 0.11		
	200			Influent	80 ± 12.2	0.55	182 ± 11.5	-1.32 ± 0.034	1.1×10-3 ± 6.5×10-4	0.024 ± 4.8×10-3
				Effluent	83 ± 58.0	0.47		-1.31 ± 0.17		
	300			Influent	129 ± 71.7	0.48	200 ± 31.5	-0.396 ± 0.21	2.4×10-3 ± 2.2×10-3	0.084 ± 7.6×10-6
				Effluent	97 ± 47.2	0.27		-0.553 ± 0.10		
	500			Influent	145 ± 30.6	0.50	236 ± 18.5	-0.567 ± 0.16	2.3×10-3 ± 1.3×10-3	0.23 ± 7.9×10-4
				Effluent	25 ± 0.9	0.56		-0.409 ± 0.032		
	1000			Influent	NM	NM	ND	NM	ND	ND
				Effluent	NM	NM		NM		
*n*CeO2		0.33		Influent	137 ± 11.5	0.34	157 ± 16.9	-2.70 ± 0.21	7.3×10-5 ± 1.4×10-4	7.3×10-3 ± 1.3×10-3
				Effluent	107 ± 11.2	0.33		-2.85 ± 0.22		
		3.3		Influent	140 ± 1.8	0.20	90 ± 9.0	-1.90 ± 0.087	6.6×10-4 ± 2.5×10-4	0.052 ± 3.1×10-3
				Effluent	136 ± 5.8	0.20		-1.88 ± 0.22		
		6.7		Influent	193 ± 8.1	0.11	106 ± 5.9	-1.44 ± 0.027	0.014 ± 5.3×10-4	0.13 ± 5.9×10-3
				Effluent	191 ± 6.8	0.12		-1.34 ± 0.023		
		8		Influent	565 ± 48.4	0.32	153 ± 15.9	-1.43 ± 0.066	0.049 ± 0.011	0.50 ± 0.47
				Effluent	487 ± 53.1	0.29		-1.40 ± 0.033		
		10		Influent	712 ± 65.3	0.92	128 ± 10.7	-1.37 ± 0.025	0.17 ± 0.12	ND
				Effluent	166 ± 16.8	0.84		-1.33 ± 0.046		
			0.33	Influent	81 ± 4.7	0.66	152 ± 8.2	-2.65 ± 0.15	1.5×10-4 ±	ND

		Effluent	93 ± 11.2	0.62		-2.54 ± 0.18	2.9×10-4
	6.7	Influent	145 ± 0.4	0.03	108 ± 14.4	-0.999 ± 0.034	0.010 ± 1.5×10-3
		Effluent	145 ± 1.0	0.04		-1.13 ± 0.069	
	8	Influent	223 ± 3.9	0.04	126 ± 4.3	-0.876 ± 0.022	0.062 ± 3.8×10-3
		Effluent	226 ± 2.5	0.03		-0.890 ± 0.030	
	12	Influent	533 ± 8.6	0.16	161 ± 17.6	-0.787 ± 0.019	0.085 ± 3.4×10-3
		Effluent	124 ± 43.7	1.00		-0.564 ± 0.092	
	7.4	Influent	80 ± 2.0	0.04	146 ± 5.3	-1.16 ± 0.030	4.0×10-3 ± 1.1×10-3	0.057 ± 9.3×10-3
		Effluent	78 ± 1.4	0.04		-1.18 ± 0.020	
*n*CAP	0.33	Influent	174 ± 33.2	0.61	92 ± 15.4	-2.26 ± 0.15	1.9×10-6 ± 3.7×10-6
		Effluent	161 ± 18.8	0.67		-2.33 ± 0.14	
	3.3†		50 ± 6.3	0.46	61 ± 3.0	-1.52 ± 0.094	ND
	6.7	Influent	116 ± 1.6	0.03	107 ± 11.3	-1.42 ± 0.062	0.013 ± 1.5×10-3
		Effluent	106 ± 1.6	0.03		-1.13 ± 0.025	
	8	Influent	111 ± 0.3	0.02	109 ± 3.0	-1.27 ± 0.038	0.011 ± 1.6×10-3	ND
		Effluent	101 ± 1.0	0.01		-1.14 ± 0.055	
	10†		207 ± 2.2	0.03	ND	-1.03 ± 0.024	ND
	16	Influent	795 ± 127.0	0.19	276 ± 22.6	-0.974 ± 0.030	0.31 ± 0.013
		Effluent	440 ± 52.3	0.51		-0.914 ± 0.024	
	20	Influent	1073 ± 91.0	0.60	392 ± 40.8	-1.04 ± 0.075	0.36 ± 0.046
		Effluent	145 ± 4.2	0.98		-0.901 ± 0.070	
	7.4	Influent	110 ± 10.0	0.02	115 ± 8.5	-0.865 ± 0.036	3.8×10-3 ± 3.0×10-3	0.085 ± 8.5×10-3
		Effluent	112 ± 7.8	0.03		-0.884 ± 0.045	

NM = This value is not reported as reproducible measurements could not be obtained.

ND = Values were not determined experimentally.

* All values represent means ± 95% CI. Effluent values determined following quartz sand column experiments.

† Column experiments were not performed.

The observed decrease in surface potential with increasing solution IS can be directly attributed to electrical double-layer compression and the screening of particle surface charge with increasing salt concentration. Compared to monovalent cations, divalent cations such as Ca^{2+} and Mg^{2+} are far more effective in masking surface charge (Hunter, 2001). While divalent cation screening efficiency results in rapid $nCeO_2$ destabilization at IS > 10 mM $CaCl_2$ or 12 mM $MgCl_2$, stable suspensions can be observed in $NaNO_3$ at IS > 500 mM. As previously suggested by Chen and Elimelech, the decrease in EPM observed in the presence of $CaCl_2$ and $MgCl_2$ may be due to the binding of Ca^{2+} and Mg^{2+} to carboxylic acid groups (Chen and Elimelech, 2007).

The zeta-potential of the quartz sand in natural and artificial groundwater matrices (pH 8) was evaluated from the measured steaming potentials. Negative zeta-potentials are observed over the range of experimental conditions, and the absolute value of the zeta-potential decreases with increasing IS, and in the presence of divalent cations. Details are provided in the Supplementary Information (Table S2).

3.2 Particle size

In this study, ENP hydrodynamic diameters were determined using DLS (d_{DLS}) and NTA (d_{NTA}). The average size of $nCeO_2$ particles in suspensions injected into the packed columns generally increases with increasing IS of $NaNO_3$, $CaCl_2$, or $MgCl_2$ (Table 1, "influent" values). Measured values of d_{DLS} range from 137 to 712 nm (in 0.33 and 10 mM $CaCl_2$, respectively), 81 to 533 nm (in 0.33 and 12 mM $MgCl_2$, respectively) and 54 to 145 nm (in 100 and 500 mM $NaNO_3$, respectively). The observed increase in $nCeO_2$ aggregate size with increasing IS is in qualitative agreement with the DLVO theory of colloid stability (Derjaguin and Landau, 1941, Verwey and Overbeek, 1948). Namely, reduced particle surface potentials at

higher IS result in decreased repulsive interaction energies between two approaching particle surfaces, giving rise to greater particle aggregation. At a given IS, nCeO$_2$ aggregate sizes are larger in CaCl$_2$ than MgCl$_2$ (Table 1). Furthermore, for the purpose of the transport studies, "stable" nCeO$_2$ suspensions could be prepared at IS of up to 12 mM MgCl$_2$; however "stable" nCeO$_2$ suspensions could not be prepared at IS > 10 mM CaCl$_2$ (suspension stability was verified by monitoring sedimentation using UV-visible spectrophotometry and changes in hydrodynamic diameter using DLS; data not shown). The aforementioned findings suggest that Ca^{2+} is more effective in masking surface charge (and compressing the polymer chains) than Mg^{2+}. This is in agreement with previous studies considering boron nanoparticle aggregation and deposition (Liu, 2009) and fullerene (C$_{60}$) aggregation (Chen and Elimelech, 2007). Both these studies found Ca^{2+} to be more effective than Mg^{2+} in screening surface charge. Finally, the measured d_{DLS} of nCeO$_2$ in natural groundwater is 80 nm (Table 1).

In addition to the particle sizing measurements performed using DLS, particle sizes for the suspensions injected into the packed columns were also measured using NTA (Table 1, d_{NTA} "influent" values). Under selected conditions, values of d_{NTA} are comparable to d_{DLS}, as noted for nCAPs in groundwater (d_{DLS}=110 nm, while d_{NTA}=115 nm). However, significant discrepancies between the two sets of measurements are at times apparent, especially at higher IS of the divalent salts, where d_{DLS} are larger than the measured d_{NTA}. DLS determined sizes for polydisperse suspensions will be biased by the larger aggregates present, as Rayleigh scattering is proportional to particle diameter raised to the 6th power (Filella et al., 1997). While NTA determined sizes are also dependant on light scattering, the masking of smaller particles in the presence of larger aggregates is less important (Domingos et al., 2009a), resulting in smaller reported diameters. Furthermore, NTA has an upper size limit on the order of 1 μm, further

decreasing reported sizes in the presence of large aggregates (Carr et al., 2008). Thus, whereas d_{DLS} for nCAPs in 20 mM CaCl$_2$ is 1073 nm (in part due to high polydispersity), d_{NTA} at this condition is 392 nm (Table 1). It should also be noted that the NTA has a lower size limit of 30 nm that is dependent on the refractive index of the nanoparticles being observed (Filipe et al., 2010). This may affect the determined sizes when examining particles with very small nominal diameters (such as the 1-10 nm particles employed herein).

The largest particle aggregates are encountered at the highest IS tested; yet, increasing the concentration of the divalent salt beyond 0.33 mM appears to result in decreased aggregate sizes in certain cases. This trend, apparent in the measured nCAP hydrodynamic sizes (d_{DLS}), as well as the d_{NTA} for nCeO$_2$ and nCAP particles suspended in divalent salts, suggests that different mechanisms may be influencing the extent of particle aggregation. While this trend is not apparent in the d_{DLS} values determined for nCeO$_2$, higher d_{DLS} standard deviations (as indicated by the 95% confidence interval) and heightened suspension polydispersity, as indicated by the polydispersity index (PDI), are encountered at the lowest (0.33 mM) divalent salt IS when compared to IS of 3.3 or 6.7 mM (Table 1). The standard deviations and PDI values observed suggest that a wider range of aggregate sizes are present at 0.33 mM than at 3.3 and 6.7 mM, where suspensions appear to be less polydisperse. The d_{DLS} of the nCAP particle at the higher IS of 3.3 and 6.7 mM CaCl$_2$ (50 and 116 nm, respectively) are also significantly smaller than the particle size at 0.33 mM (174 nm), where heightened polydispersity is again encountered. As observed with nCeO$_2$, nCAP size increases at the highest IS (Table 1).

It is known that PAA can adopt different conformations based on surrounding solvent characteristics such as the ion species present, pH and IS (Turro and Arora, 1986). Whereas a coiled, more compressed conformation may be favored when carboxylic acid groups are

17

protonated (due to hydrogen bonding between monomers), deprotonation will result in electrostatic repulsion within the PAA backbone, favoring a stretched conformation (Sarkar and Somasundaran, 2004). Likewise, while repulsive interactions between charged carboxyl groups will result in extended PAA conformations at lower IS, the addition of counterions (i.e. increased IS) will screen the charge, enabling the polyelectrolyte chains to collapse (Coulter et al., 2010). Partial crosslinking of the PAA chains by the manufacturer also likely affects the extent of PAA expansion and compression.

The fact that PAA can adopt different conformations is likely responsible for the larger particle sizes or heightened polydispersity observed at the lowest (0.33 mM) divalent salt IS, as a stretched polymer conformation is favored. Under these conditions, the extended polymer chains contribute to the larger particle size detected. Increasing the IS leads to decreased repulsion within the PAA polymer chains, enabling them to become more coiled, compressed and uniform (as polymer chains are fastened in place by the divalent counterions). This corresponds to the decrease in recorded size and/or PDI as IS increases to 3.3 or 6.7 mM. Decreased electrostatic repulsion and reduced steric effects (due to polymer compression) will ultimately favor particle aggregation, resulting in the formation of the larger aggregates observed at the highest salt concentrations examined. The influence of solution IS on the thickness of nanoparticle polymer coatings is currently the focus of ongoing research in our group.

While nCAP composition is analogous to that of the nCeO$_2$ polymer coating, nCAP aggregate sizes are generally smaller than nCeO$_2$ at a given CaCl$_2$ IS (Table 1). For instance, the d_{DLS} of nCeO$_2$ in 8 mM CaCl$_2$ is 565 nm, whereas nCAP aggregates at this IS measure 111 nm. Due to the heightened nCeO$_2$ aggregation observed, stable ceria suspensions can not be prepared at IS above 10 mM CaCl$_2$. On the other hand, nCAP suspensions can be prepared at IS as high

as 20 mM $CaCl_2$. The greater nCeO$_2$ aggregation suggests that the polymer coating on this particle may not be completely uniform and, hence, may not provide as effective electrosteric stabilization as that observed for the nCAP. The pH$_{zpc}$ for bare nCeO$_2$ is reported to be pH 7.6 (Li et al., 2011a). As previously observed with natural organic matter adsorbed on the surface of metal oxide particles (Domingos et al., 2009b, Kretzschmar et al., 1997), the PAA coating in this study significantly alters the particle surface potential, as the pH$_{zpc}$ for the nCeO$_2$ particles employed is below pH 2 (Figure S2). Given that all experiments are conducted at pH 8 (~pH$_{zpc}$ for the nCeO$_2$ core), any exposed nCeO$_2$ core material carries virtually no surface charge. The nCeO$_2$ particles with partially exposed cores will be more likely to aggregate, as weaker repulsive forces are encountered at the uncovered sites. This phenomenon is not an issue for the nCAPs, as they consist solely of PAA.

3.3 Transport and deposition of nCeO$_2$ and nCAP

The primary aim of this study is to investigate nCeO$_2$ and nCAP deposition behavior in quartz sand and loamy sand-packed columns. ENP transport studies were conducted using natural groundwater or artificial solutions of either monovalent (NaNO$_3$) or divalent (CaCl$_2$, MgCl$_2$) salts. Given the aforementioned discrepancies between the two particle sizing techniques, both d_{DLS} and d_{NTA} values were considered in calculating the single-collector contact efficiency (η_0), resulting in two estimates for the ENP attachment efficiency, α (using eq 1). Furthermore, for each transport experiment, the normalized particle concentration at the column effluent (C/C_0) was evaluated using two approaches: (i) averaging values between 1.8-2 PVs and, (ii) by numerical integration of the area under each breakthrough curve. Consequently, for each experimental condition, four distinct α values were obtained. Regardless of the sizing technique

19

and manner in which C/C_0 is determined, the calculated α values are within a factor of 1-3 times for the vast majority of experimental conditions (Tables S3 and S4). For simplicity, attachment efficiencies discussed herein and presented in Table 1 are those obtained using d_{DLS} and C/C_0 values evaluated by numerical integration of the particle breakthrough curves.

3.3.1. Transport and deposition in the presence of monovalent salts

Regardless of [NaNO$_3$] (IS ranging from 0.1 to 1 M), virtually all nCeO$_2$ particles elute from the quartz sand-packed columns (Figure 1a). Even at 1 M IS, only 20% retention is observed. Given that particle and collector surfaces are negatively charged at pH 8, lower absolute surface potentials at higher IS should render deposition more favorable, while heightened aggregation could result in the physical straining of particles within the packed column. Although particle EPM decreases (-1.1 to -0.57 μmcmV^{-1}s^{-1}) and aggregate size increases (54 to 145 nm) when the IS increases from 100 to 500 mM NaNO$_3$ (Table 1), near complete particle elution is still observed over this range of IS. Nonetheless, comparison of nCeO$_2$ particle sizes in column influent and effluent suspensions provides support for a mechanism of particle straining (Table 1). Physical straining occurs when large aggregates become entrapped in the narrower pores between collector surfaces (Bradford et al., 2002, Shen et al., 2008). As the pores clog, incoming particles become entrapped, resulting in decreased elution. The data in Table 1 show that, at IS > 200 mM NaNO$_3$, nCeO$_2$ particle sizes in the column effluent are considerably smaller than those measured in the influent suspensions. This suggests that the larger aggregates formed at the higher salt concentrations are preferentially retained in the granular matrix (likely by physical straining).
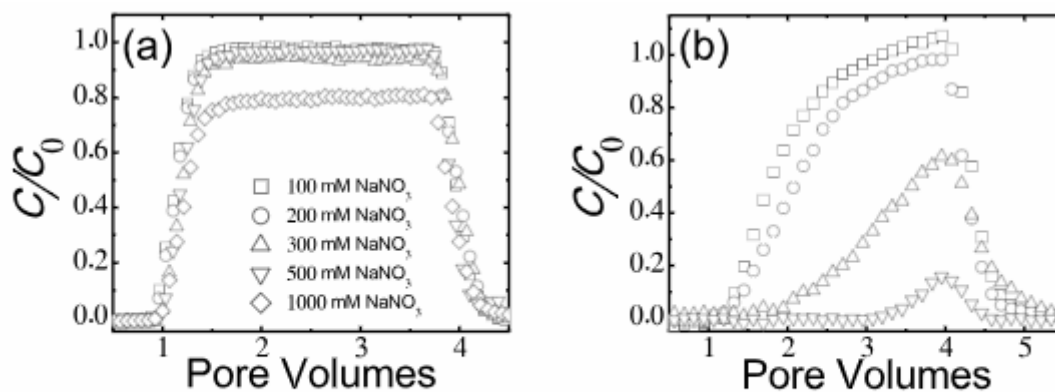
Fig. 1 – nCeO$_2$ breakthrough curves in NaNO$_3$. Transport experiments were performed in (a) quartz and (b) loamy sand-packed columns using 100 mg/L nCeO$_2$ suspensions (pH 8).

Significantly more retention is reported in a recent study by Li *et al.* (Li et al., 2011b) investigating bare nCeO$_2$ transport and deposition in 45 cm sand-packed columns. Although the particles used in their study were suspended in monovalent NaCl, significant particle retention occurred at 1 mM IS under more favorable deposition conditions (pH 3) and at 10 mM IS under unfavorable deposition conditions (pH 6 and pH 9). While the longer columns employed by Li *et al.* would naturally result in greater particle retention, they also made use of coarser quartz sand (d=717 μm) and a faster 20 mL/min flow rate (Li et al., 2011b). Hence, the observed discrepancies between the two studies are likely due to the PAA coating on the Vive Crop Protection^{TM} particles. Such a coating can result in the electrosteric stabilization of the particles (Elimelech et al., 1995, Franchi and O'Melia, 2003), resulting in heightened particle transport.

Liu *et al.* (Liu et al., 2012) also report very high retention of bare nCeO$_2$ in quartz sand-packed columns (10 mM NaCl). While their columns were similar in length and contained collector grains of similar composition and size (sand sifted through 250–300 μm sieves) to those used herein, only 4.3% of nCeO$_2$ was found to elute at pH 8.5 in their study. The nCeO$_2$ employed by Liu *et al.* had a pH$_{zpc}$ of 6.8, rendering deposition unfavorable at pH 8.5. The

21

authors suggest that heightened retention under unfavorable conditions may have resulted from surface roughness and chemical heterogeneities on the collector surfaces (Liu et al., 2012). In the presence of organic matter (e.g., humic acid), they observed enhanced nCeO$_2$ stability and mobility (in 1 mM NaCl, pH 6.5), likely due to electrosteric effects of the adsorbed humic acid. Adding 1, 3 or 6 mg/L humic acid, resulted in increased particle elution. The heightened particle elution observed in the presence of stabilizing humic acid (Liu et al., 2012) is in better agreement with the polymer-coated nCeO$_2$ transport observed in the present study (in NaNO$_3$).

When nCeO$_2$ particles suspended in NaNO$_3$ are added to loamy sand-packed columns, greater particle retention is observed, with α values as high as 0.23 at 500 mM IS (Table 1). In contrast to the steady-state behavior observed in the quartz sand columns (Figure 1a), particle elution is dynamic and increases over time in the loamy sand (Figure 1b). The heightened retention observed in loamy sand is likely due to increased favorable deposition sites within the packed bed when compared to quartz sand. These additional sites likely result from the presence of clays within the loamy sand (Quevedo and Tufenkji, 2012). While albite (pH$_{zpc}\approx$5.9) and orthoclase (pH$_{zpc}\approx$1) in the clay fraction present unfavorable conditions for nCeO$_2$ and nCAP retention at pH 8, allophane (pH$_{zpc}\approx$7.8) in the clay fraction may provide additional positively charged sites onto which negatively charged ENPs can "favorably" deposit (Quevedo and Tufenkji, 2012, Sposito, 1989). Although the Fe content of the loamy sand was not quantified, the presence of Fe was confirmed by EDS. If iron oxides are present in the loamy sand, they would also play an important role in the favorable deposition of the negatively charged ENPs (Ryan and Elimelech, 1996).

The number of favorable deposition sites in the packed bed increases with increasing IS due to the charge masking effect of the Na$^+$ counterions. This leads to increased retention with

increasing IS within the loamy sand (Figure 1b). The dynamic elution behavior observed is indicative of a blocking effect within the column (Liu et al., 1995, Ryan and Elimelech, 1996). As favorable deposition sites become occupied, fewer sites remain for incoming particles. Thus, the incoming particles are repelled by deposited particles with similar surface potentials and less likely to find an available deposition site. Electrostatic repulsion and steric interactions may also prevent incoming particles from depositing onto sites adjacent to previously deposited particles (Ko and Elimelech, 2000). These conditions result in increased particle elution over time. Although the size of nCeO$_2$ particles in the column effluent were not measured for experiments conducted with loamy sand packed columns, it is very likely that physical straining also contributes to the retention of particles in this system. The extent of physical straining is strongly influenced by the particle to grain size ratio (Tufenkji et al., 2004); because the mean sizes of the two sands are comparable, there is a strong possibility that straining is also playing a role in the loamy sand.

3.3.2. Transport and deposition in the presence of divalent salts

In the presence of divalent salts, the attachment efficiency increases over several orders of magnitude with increasing IS (Table 1). For nCeO$_2$ suspended in CaCl$_2$ (0.33 to 10 mM), determined α values range from 7.3×10^{-5} to 0.17 in quartz sand, and 7.3×10^{-3} to 0.50 in loamy sand (Table 1). Likewise, nCeO$_2$ attachment efficiency in quartz sand increases from 1.5×10^{-4} to 0.085 when the IS of MgCl$_2$ is increased from 0.33 to 12 mM (Table 1). While dynamic (time-dependent) particle transport behavior is encountered in both granular materials, less retention is observed in the quartz sand at any given IS.

In quartz sand, significant particle retention is observed at CaCl$_2$ IS $\geq$ 6.7 mM (Figure 2a). At pH 8, the nCeO$_2$ and quartz sand have a negative surface potential, rendering deposition unfavorable. Nonetheless, the particle and collector surface potentials observed at 6.7 mM CaCl$_2$ are less negative than at 0.33 mM CaCl$_2$ (Table S2). Such decreased surface potentials increase the likelihood of deposition as electrostatic particle-surface interactions are less repulsive (Derjaguin and Landau, 1941, Elimelech and O'Melia, 1990a, b, Verwey and Overbeek, 1948). Furthermore, as discussed previously, higher [CaCl$_2$] will decrease electrostatic repulsion within the PAA coating, favoring a compressed conformation. This will result in decreased steric repulsion, further favoring particle deposition. Slightly more than 20% of particles suspended in 6.7 mM CaCl$_2$ are retained by the quartz sand, with elution increasing over time (due to the aforementioned blocking phenomenon). On the other hand, 75% of the nCeO$_2$ is retained in loamy sand at the same IS (Figure 2b).

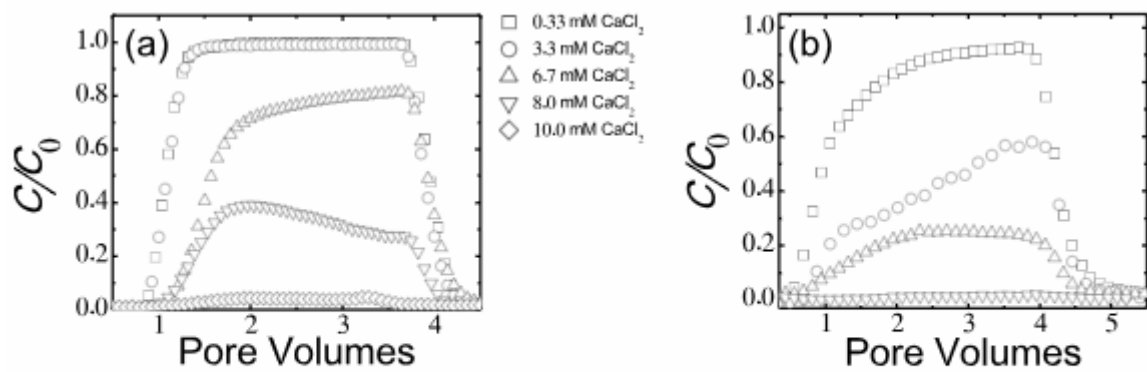Fig. 2 – nCeO$_2$ breakthrough curves in CaCl$_2$. Transport experiments were performed in (a) quartz and (b) loamy sand-packed columns using 100 mg/L nCeO$_2$ suspensions (pH 8).

It is interesting to note that at 8 mM IS CaCl$_2$, the elution of nCeO$_2$ particles decreases with time (Figure 2a). At this condition, the nCeO$_2$ particles are larger than those observed at lower [CaCl$_2$] (565 nm versus 193 nm at 6.7 mM), suggesting the decreased particle elution with time could be a result of physical straining. Here, influent and effluent values of d_{DLS} for

nCeO$_2$ are generally comparable at the lower concentrations of CaCl$_2$ (Table 1), indicating that particle aggregation or particle straining do not occur during the transport experiment. Yet, at higher CaCl$_2$ concentrations, nCeO$_2$ particle sizes in the column effluent are consistently smaller than influent values, suggesting that physical straining occurs. In 8 mM CaCl$_2$, the effluent d_{DLS} (487 nm) is significantly smaller than the influent d_{DLS} (565 nm). This is even more apparent in 10 mM CaCl$_2$, where the influent d_{DLS} (712 nm) is considerably larger than the effluent diameter (166 nm). While blocking of the most favorable deposition sites is likely occurring, physical straining is likely responsible for the observed decreased particle elution with time at higher IS.

As observed in CaCl$_2$, nCeO$_2$ particles suspended in MgCl$_2$ exhibit heightened deposition at higher IS in quartz sand (Figure 3). However, contrary to the physical straining observed at 8 and 10 mM CaCl$_2$ (Figure 2a), blocking is apparent at MgCl$_2$ IS ranging from 6.7 to 12 mM, with particle elution increasing over time (Figure 3). The distinct dynamic behaviors observed likely result from differences in the aggregate sizes encountered in the two divalent salts. Overall, aggregates in the MgCl$_2$ solutions are smaller than in CaCl$_2$ at a given IS. At 8 mM IS, the nCeO$_2$ d_{DLS} in MgCl$_2$ is 223 nm, which is significantly smaller than the 565 nm d_{DLS} measured in 8 mM CaCl$_2$ (Table 1). It appears the smaller aggregates in MgCl$_2$ do not result in the significant physical straining observed at higher CaCl$_2$ IS. Consequently, once favorable deposition sites become occupied, heightened particle elution is observed. At the highest MgCl$_2$ IS tested (12 mM), aggregate sizes are much larger (533 nm). Furthermore, effluent d_{DLS} are much smaller than influent d_{DLS}, suggesting that the largest aggregates are preferentially retained (Table 1). The fact that this does not result in significant physical straining (based on the slope of the breakthrough curves, Figure 3) suggests there are likely fewer large aggregates in the

MgCl$_2$ solutions. Although the largest may become entrapped in the packed bed, their retention

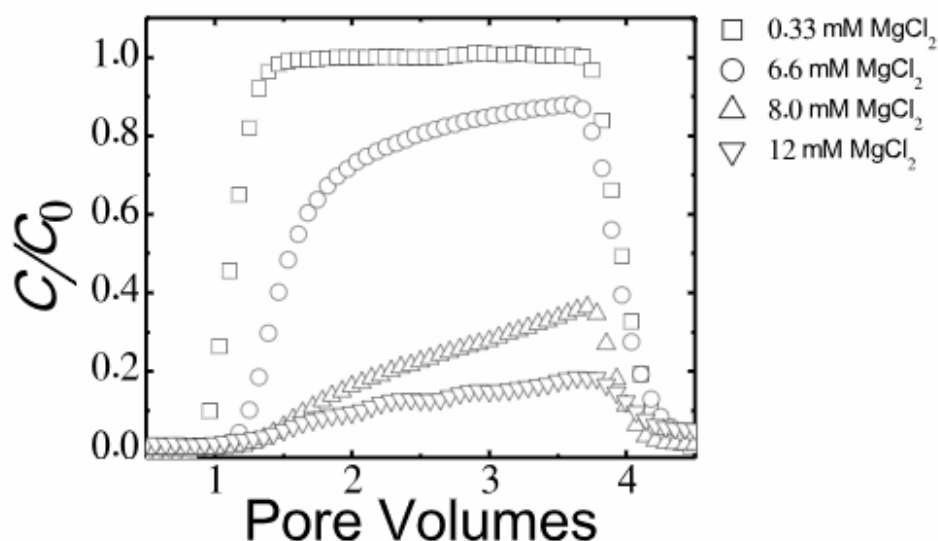does not appear to result in the extensive pore clogging and physical straining observed in CaCl$_2$.

Fig. 3 – nCeO$_2$ breakthrough curves in MgCl$_2$. Transport studies were performed in quartz sand using 100 mg/L nCeO$_2$ suspensions (pH 8).

The transport and deposition behavior of the nCAPs, consisting of the same PAA

polymer that is present on the nCeO$_2$ particle surface, was also examined under selected

conditions. The water dispersible nCAPs are among various prototypes developed by Vive Crop

Protection to potentially deliver active agents that protect crops and heighten yields, while

decreasing the use of potentially harmful pesticides. Before such capsules can be applied to

agricultural soils on a large scale, their behavior in model subsurface environments must be

evaluated.

Similar to the trends observed for nCeO$_2$, the nCAP breakthrough curves also exhibit

increased retention with increasing [CaCl$_2$] in quartz sand (Figure 4). Moreover, increased

nCAP elution with time (indicative of particle blocking) is observed at 6.7 and 8.0 mM CaCl$_2$.

As observed with nCeO$_2$, the d_{DLS} of the nCAP in column effluent suspensions is smaller than

the measured hydrodynamic diameter of the influent suspensions at higher CaCl$_2$ IS (Table 1).

26

For example, at 16 mM IS, the influent d_{DLS} (795 nm) is nearly twice as large as the size of the

nCAPs in the column effluent. These data suggest that larger aggregates are preferentially

retained within the granular medium. nCAP attachment efficiencies are comparable to the

nCeO$_2$ α values observed in 6.7 and 8 mM CaCl$_2$ and in natural groundwater (Table 1),

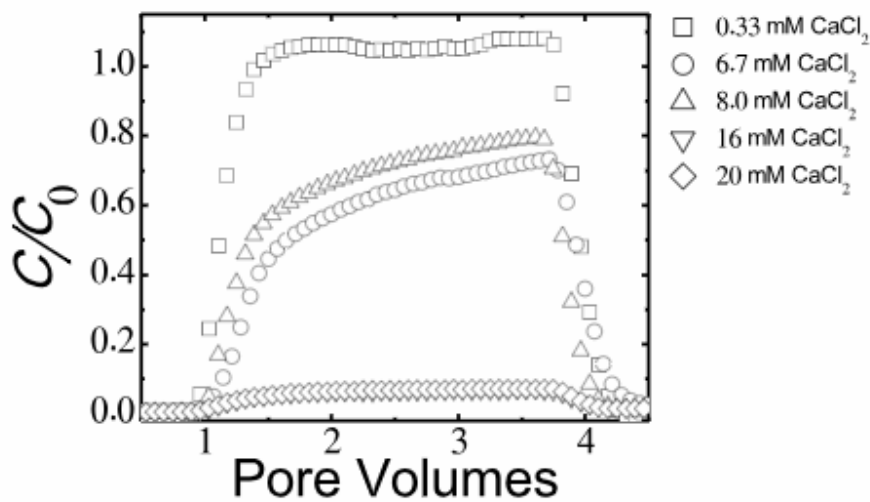suggesting the two particle types have a similar transport potential.

Figure 4. Representative breakthrough curves for nCAP particles in quartz sand-packed columns (0.33 – 20 mM CaCl$_2$, pH 8).

3.3.3. Transport and deposition of ENPs suspended in a natural groundwater

In quartz sand, nCeO$_2$ and nCAP particles suspended in natural groundwater

demonstrate significant transport potential, with particle elution gradually approaching 80 and

100%, respectively (Figure 5a). While the attachment efficiency for both particle types is

approximately 4×10^{-3} in quartz sand, calculated α values are an order of magnitude larger in

loamy sand (Table 1). A previous study conducted in our laboratory also showed QD and

carboxylated polystyrene latex nanoparticle retention in loamy sand to be heightened by an order

of magnitude compared to particle behavior in quartz sand (Quevedo and Tufenkji, 2012). The

shapes of the particle breakthrough curves from experiments conducted using the loamy sand

columns and natural groundwater indicate that particle blocking contributes to the overall nCeO$_2$ and nCAP transport behavior (Figure 5b). As observed in quartz sand, the transport potential for both particles in loamy sand is very similar, with α values of 0.057 and 0.085 for nCeO$_2$ and nCAP, respectively. In contrast, our group previously observed that the retention behaviors of two carboxy-terminated QDs and a carboxylated polystyrene latex nanoparticle were distinct in loamy sand (Quevedo and Tufenkji, 2012). Although the coatings of all three particle types in the aforementioned study possessed carboxyl functional groups, their surfaces consisted of different polymers. Consequently, variations in transport behavior likely resulted from differences in polymer-coating affinities for specific loamy sand components. Such apparent differences were not encountered in the present study, as nCAP particle composition is analogous to the nCeO$_2$ polymer coating.
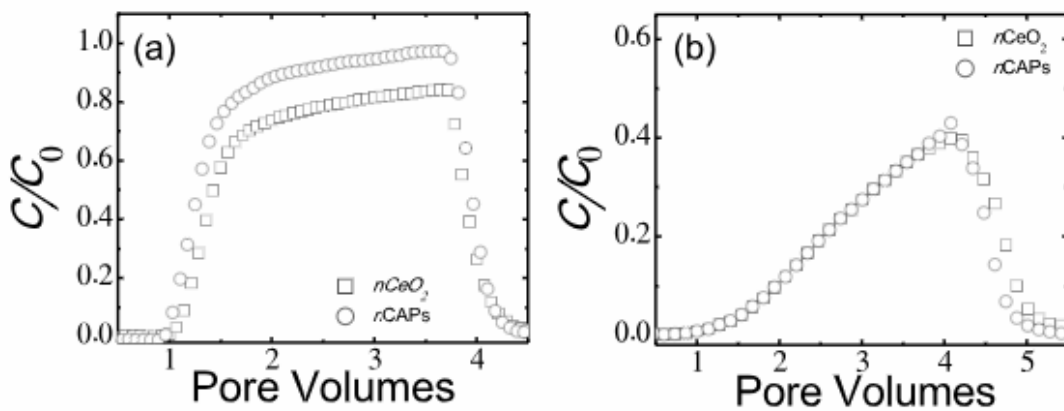

Figure 5. Representative breakthrough curves for nCAP and nCeO$_2$ particles suspended in natural groundwater and injected into (a) quartz sand and (b) loamy sand-packed columns (pH 8).

The natural groundwater used in this study has a total IS of 7.4 mM, of which Ca^{2+} and Mg^{2+} account for 5 mM (3.6 mM Ca^{2+} and 1.4 mM Mg^{2+}). Thus, it is of interest to compare the transport of the ENPs in the artificial matrices having comparable concentrations of the divalent cations. In quartz and loamy sands, nCeO$_2$ attachment efficiencies observed in natural groundwater are higher than those observed in 3.3 mM CaCl$_2$ and lower than those observed at

6.7 mM CaCl$_2$. These findings correspond to the fact that divalent cations account for 5 mM of the total 7.4 mM groundwater IS. Likewise, in quartz sand, the nCAP α value observed in natural groundwater is lower than that observed in 6.7 mM CaCl$_2$.

3.3.4. Summary of the transport behavior of PAA-coated ENPs

One of the aims of this study is to compare nCeO$_2$ and nCAP transport behavior. When plotting nCeO$_2$ and nCAP particle attachment efficiencies in quartz sand as a function of CaCl$_2$ IS (Figure 6), it is evident that nCAP α values are smaller at 0.33 mM and comparable to nCeO$_2$ at 6.7 and 8 mM. Beyond the current study, previous work by this group considered the transport behavior of nTiO$_2$, nZnO and CdTe QDs with the same PAA-derived surface coating (Petosa et al., 2012, Quevedo and Tufenkji, 2012). As in the current study, we also observed that α increases with increasing IS for the other PAA-coated ENPs. In Figure 6, we have included previously reported α values for experiments conducted with the PAA-coated nTiO$_2$, nZnO and CdTe QDs in CaCl$_2$ and quartz sand. The attachment efficiencies for these other ENPs are generally higher than those observed with the nCAP (Figure 6). At 8 mM CaCl$_2$, the nCAP α in quartz sand is 0.011, orders of magnitude smaller than the α values previously observed for nTiO$_2$ (α=0.63) and nZnO (α=1.1) (Petosa et al., 2012). Likewise, α=0.69 for QDs in 5 mM CaCl$_2$ (Quevedo and Tufenkji, 2012), which is higher than the nCAP attachment efficiency at 20 mM IS. The data in Figure 6 demonstrate that while the transport behavior for the various particle types is not identical (potentially due to partially exposed cores), the nCAP transport behavior is most comparable to that of the nCeO$_2$ particles. Note that while nCAP, nCeO$_2$ and nZnO studies were conducted at pH 8, nTiO$_2$ and QD studies were conducted at pH 7.

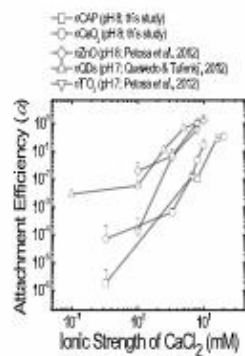Figure 6. Attachment efficiency (α) as a function of CaCl$_2$ IS for nCAP, nCeO$_2$, QD, nTiO$_2$ and nZnO particles in quartz sand-packed columns.

While the current study improves our understanding of nCeO$_2$ transport and deposition behavior in saturated granular environments, there are inherent limitations that should be noted. Firstly, soil characteristics (e.g., hydraulic conductivity, mineralogical and organic matter content) are location and depth dependent. Consequently, ENP affinity for various soil types and in different soil horizons will vary significantly. Nonetheless, the current study identifies particular environmental characteristics that result in enhanced ENP mobility (e.g., sandy soils, lower salt concentrations). Furthermore, while different natural and artificial groundwater matrices are employed, all experiments are conducted at pH 8. Geographical variations in groundwater pH will affect ENP deposition as changes in particle and collector surface potential, colloidal stability, aggregate size and interactions with soil components (e.g., humic substances) will occur (Navarro et al., 2009, Quevedo and Tufenkji, 2012). Finally, the loamy sand packed-columns employed are not extracted as undisturbed cores. Still, by conducting well-controlled experiments using two different granular materials, we obtain useful insight into the influence of collector grain properties and water chemistry on ENP transport and retention.

4. Conclusions

This study clearly demonstrates that it is necessary to consider aquatic matrix composition and soil type in evaluating ENP contamination risks. Overall, enhanced $nCeO_2$ particle retention is encountered at higher divalent salt ($CaCl_2$ and $MgCl_2$) concentrations and in loamy sand. Namely, it is evident that:

- while virtually all $nCeO_2$ particles suspended in $[NaNO_3] \leq 500$ mM elute from the quartz sand-packed columns, heightened particle retention and dynamic behavior (blocking) is observed in loamy sand.

- $nCeO_2$ attachment efficiency increases over several orders of magnitude within a narrow range of divalent salt IS (0.33–10 mM $CaCl_2$ and 1–12 mM $MgCl_2$). While dynamic behavior (blocking and physical straining) is encountered in both granular materials, lower retention is observed in quartz sand at any given IS.

- $nCeO_2$ and $nCAP$ attachment efficiencies for particles suspended in natural groundwater are an order of magnitude higher in loamy sand than in quartz sand.

- the enhanced retention observed in loamy sand may partially be due to the presence of favorable deposition sites on clays such as allophane, and metal oxides such as iron oxide.

The aforementioned findings indicate that specific environmental conditions (e.g., sandy soils, decreased ionic strength, and decreased divalent salt concentrations) are more conducive to heightened particle mobility. Finally, the transport potential of the model polymeric capsule ($nCAP$) is generally greater than that of various PAA-coated ENPs previously tested and most comparable to the $nCeO_2$ used in the present study.

Acknowledgements

References

Auffan, M., Rose, J., Bottero, J.-Y., Lowry, G.V., Jolivet, J.-P. and Wiesner, M.R., 2009. Towards a definition of inorganic nanoparticles from an environmental, health and safety perspective. Nature Nanotechnology 4, 634-641.

Bradford, S.A., Yates, S.R., Bettahar, M. and Simunek, J., 2002. Physical factors affecting the transport and fate of colloids in saturated porous media. Water Resources Research 38 (12), 631-6312.

Carr, B., Malloy, A. and Warren, J., 2008. Nanoparticle tracking analysis. Innovations in Pharmaceutical Technology (26), 38-40.

Cassee, F.R., Van Balen, E.C., Singh, C., Green, D., Muijser, H., Weinstein, J. and Dreher, K., 2011. Exposure, health and ecological effects review of engineered nanoscale cerium and cerium oxide associated with its use as a fuel additive. Critical Reviews in Toxicology 41 (3), 213-229.

Chen, K.L. and Elimelech, M., 2007. Influence of humic acid on the aggregation kinetics of fullerene (C_{60}) nanoparticles in monovalent and divalent electrolyte solutions. Journal of Colloid and Interface Science 309 (1), 126-134.

Coulter, M.M., Dinglasan, J.A., Goh, J.B., Nair, S., Anderson, D.J. and Dong, V.M., 2010. Preparing water-dispersed palladium nanoparticles via polyelectrolyte nanoreactors. Chemical Science 1 (6), 772-775.

Derjaguin, B.V. and Landau, L.D., 1941. Theory of stability of strongly charged lyophobic sols and the adhesion of strongly charged particles in solutions of electrolytes. Acta Physicochimica URSS 14, 633-662.

Domingos, R.F., Baalousha, M.A., Ju-Nam, Y., Reid, M.M., Tufenkji, N., Lead, J.R., Leppard, G.G. and Wilkinson, K.J., 2009a. Characterizing manufactured nanoparticles in the environment: Multimethod determination of particle sizes. Environmental Science & Technology 43 (19), 7277-7284.

Domingos, R.F., Tufenkji, N. and Wilkinson, K.J., 2009b. Aggregation of titanium dioxide nanoparticles: Role of a fulvic acid. Environmental Science and Technology 43 (5), 1282-1286.

Elimelech, M., Gregory, J., Jia, X. and Williams, R.A., 1995. Particle Deposition and Aggregation: Measurement, Modeling, and Simulation, Butterworth-Heinemann, Oxford.

Elimelech, M. and O'Melia, C.R., 1990a. Effect of particle size on collision efficiency in the deposition of brownian particles with electrostatic energy barriers. Langmuir 6 (6), 1153-1163.

Elimelech, M. and O'Melia, C.R., 1990b. Kinetics of deposition of colloidal particles in porous media. Environmental Science and Technology 24 (10), 1528-1536.

Filella, M., Zhang, J., Newman, M.E. and Buffle, J., 1997. Analytical applications of photon correlation spectroscopy for size distribution measurements of natural colloidal suspensions: Capabilities and limitations. Colloids and Surfaces A: Physicochemical and Engineering Aspects 120 (1-3), 27-46.

Filipe, V., Hawe, A. and Jiskoot, W., 2010. Critical evaluation of nanoparticle tracking analysis (NTA) by NanoSight for the measurement of nanoparticles and protein aggregates. Pharmaceutical Research 27 (5), 796-810.

Franchi, A. and O'Melia, C.R., 2003. Effects of natural organic matter and solution chemistry on the deposition and reentrainment of colloids in porous media. Environmental Science and Technology 37 (6), 1122-1129.

García, A., Espinosa, R., Delgado, L., Casals, E., González, E., Puntes, V., Barata, C., Font, X. and Sánchez, A., 2011. Acute toxicity of cerium oxide, titanium oxide and iron oxide nanoparticles using standardized tests. Desalination 269 (1-3), 136-141.

Hunter, R.J., 2001. Foundations of Colloid Science, Oxford University Press Inc., New York.

Jaisi, D.P. and Elimelech, M., 2009. Single-walled carbon nanotubes exhibit limited transport in soil columns. Environmental Science and Technology 43 (24), 9161-9166.

Johnson, A.C. and Park, B., 2012. Predicting contamination by the fuel additive cerium oxide engineered nanoparticles within the United Kingdom and the associated risks. Environmental Toxicology and Chemistry.

Ju-Nam, Y. and Lead, J.R., 2008. Manufactured nanoparticles: An overview of their chemistry, interactions and potential environmental implications. Science of the Total Environment 400 (1-3), 396-414.

Keller, A.A., Wang, H., Zhou, D., Lenihan, H.S., Cherr, G., Cardinale, B.J., Miller, R. and Zhaoxia, J.I., 2010. Stability and aggregation of metal oxide nanoparticles in natural aqueous matrices. Environmental Science and Technology 44 (6), 1962-1967.

Klaine, S.J., Alvarez, P.J.J., Batley, G.E., Fernandes, T.F., Handy, R.D., Lyon, D.Y., Mahendra, S., McLaughlin, M.J. and Lead, J.R., 2008. Nanomaterials in the environment: Behavior, fate, bioavailability, and effects. Environmental Toxicology and Chemistry 27 (9), 1825-1851.

Ko, C.H. and Elimelech, M., 2000. The 'shadow effect' in colloid transport and deposition dynamics in granular porous media: Measurements and mechanisms. Environmental Science and Technology 34 (17), 3681-3689.

Kretzschmar, R., Barmettler, K., Grolimund, D., Yan, Y.D., Borkovec, M. and Sticher, H., 1997. Experimental determination of colloid deposition rates and collision efficiencies in natural porous media. Water Resources Research 33 (5), 1129-1137.

Kretzschmar, R., Robarge, W.P. and Amoozegar, A., 1994. Filter efficiency of three saprolites for natural clay and iron oxide colloids. Environmental Science and Technology 28 (11), 1907-1915.

Li, K., Zhang, W., Huang, Y. and Chen, Y., 2011a. Aggregation kinetics of CeO_2 nanoparticles in KCl and $CaCl_2$ solutions: Measurements and modeling. Journal of Nanoparticle Research 13 (12), 6483-6491.

Li, Z., Sahle-Demessie, E., Hassan, A.A. and Sorial, G.A., 2011b. Transport and deposition of CeO_2 nanoparticles in water-saturated porous media. Water Research 45 (15), 4409-4418.

Liu, D., Johnson, P.R. and Elimelech, M., 1995. Colloid deposition dynamics in flow through porous media: Role of electrolyte concentration. Environmental Science and Technology 29 (12), 2963-2973.

Liu, X., Chen, G. and Su, C., 2012. Influence of collector surface composition and water chemistry on the deposition of cerium dioxide nanoparticles: QCM-D and column experiment approaches. Environmental Science and Technology 46 (12), 6681-6688.

Liu, X., Wazne, M., Christodoulatos, C., Jasinkiewicz, K.L., 2009. Aggregation and deposition behavior of boron nanoparticles in porous media. Journal of Colloid and Interface Science 330 (1), 90-96.

Navarro, D.A.G., Watson, D.F., Aga, D.S. and Banerjee, S., 2009. Natural organic matter-mediated phase transfer of quantum dots in the aquatic environment. Environmental Science and Technology 43 (3), 677-682.

Pelley, A.J. and Tufenkji, N., 2008. Effect of particle size and natural organic matter on the migration of nano- and microscale latex particles in saturated porous media Journal of Colloid and Interface Science 321 (1), 74-83.

Petosa, A.R., Brennan, S.J., Rajput, F. and Tufenkji, N., 2012. Transport of two metal oxide nanoparticles in saturated granular porous media: Role of water chemistry and particle coating. Water Research 46 (4), 1273-1285.

Petosa, A.R., Jaisi, D.P., Quevedo, I.R., Elimelech, M. and Tufenkji, N., 2010. Aggregation and deposition of engineered nanomaterials in aquatic environments: Role of physicochemical interactions. Environmental Science and Technology 44 (17), 6532-6549.

Quevedo, I.R. and Tufenkji, N., 2012. Mobility of functionalized quantum dots and a model polystyrene nanoparticle in saturated quartz sand and loamy sand. Environmental Science and Technology 46 (8), 4449-4457.

Ryan, J.N. and Elimelech, M., 1996. Colloid mobilization and transport in groundwater. Colloids and Surfaces A: Physicochemical and Engineering Aspects 107, 1-56.

Sarkar, D. and Somasundaran, P., 2004. Conformational dynamics of poly (acrylic acid). A study using surface plasmon resonance spectroscopy. Langmuir 20 (11), 4657-4664.

Shen, C., Huang, Y., Li, B. and Jin, Y., 2008. Effects of solution chemistry on straining of colloids in porous media under unfavorable conditions. Water Resources Research 44 (W05419), 1-12.

Sposito, G., 1989. The Chemistry of Soils, Oxford University Press, Inc., New York.

Tufenkji, N. and Elimelech, M., 2004. Correlation equation for predicting single-collector efficiency in physicochemical filtration in saturated porous media. Environmental Science and Technology 38 (2), 529-536.

Tufenkji, N., Miller, G.F., Ryan, J.N., Harvey, R.W. and Elimelech, M., 2004. Transport of *Cryptosporidium* oocysts in porous media: Role of straining and physicochemical filtration. Environmental Science and Technology 38 (22), 5932-5938.

Turro, N.J. and Arora, K.S., 1986. Pyrene as a photophysical probe for intermolecular interactions of water-soluble polymers in dilute solutions. Polymer 27 (5), 783-796.

Van Hoecke, K., De Schamphelaere, K.A.C., Van der Meeren, P., Smagghe, G. and Janssen, C.R., 2011. Aggregation and ecotoxicity of CeO_2 nanoparticles in synthetic and natural waters with variable pH, organic matter concentration and ionic strength. Environmental Pollution 159 (4), 970-976.

Verwey, E.J.W. and Overbeek, J.T.G., 1948. Theory of the Stability of Lyophobic Colloids, Elsevier, Amsterdam.

Wiesner, M.R. and Bottero, J.-Y., 2007. Environmental Nanotechnology, The McGraw-Hill Companies, New York.

Yao, K.M., Habibian, M.T. and O'Melia, C.R., 1971. Water and waste water filtration: Concepts and applications. Environmental Science and Technology 5 (11), 1105-1112.

Graphical Abstract

Transport Potential of PAA-coated nCeO$_2$

nCeO$_2$ Transport in Quartz Sand $\gg$ nCeO$_2$ Transport in Loamy Sand